The computational route from bilayer membranes to vesicle fusion

Julian C Shillcock and Reinhard Lipowsky

Max Planck Institute of Colloids and Interfaces, 14424 Potsdam, Germany[1]

Abstract
Biological membranes are examples of 'smart' materials whose properties and behaviour emerge from the propagation across many scales of the molecular characteristics of their constituents. Artificial smart materials, such as drug delivery vehicles and biosensors, often rely on modifying naturally occurring soft matter, such as polymers and lipid vesicles, so that they possess useful behaviour. However, the complexity of natural membranes, both in their static properties, exemplified in their phase behaviour, and in their dynamic properties, as in the kinetics of their formation and interactions, hinders their rational modification. Mesoscopic simulations, such as dissipative particle dynamics (DPD), allow *in silico* experiments to be easily and cheaply performed on complex, soft materials requiring as input only the molecular structure of the constituents at a coarse-grained level. They can therefore act as a guide to experimenters prior to performing costly assays. Additionally, mesoscopic simulations provide the only currently feasible window on the length- and timescales relevant to important biophysical processes such as vesicle fusion. We review here the development of computational models of bilayer membranes, and in particular the use of mesoscopic simulations to follow the molecular rearrangements that occur during membrane fusion.

1. Introduction

The desire to understand natural phenomena is driven both by curiosity and economics. In the field of *soft materials*, chemists want to know how the molecular structure of reactants influences their behaviour. Materials scientists seek to learn how the molecular properties of their constituents combine to yield a material's macroscopic properties. Biologists would like to understand how a cell interacts with its environment, taking in nutrients, repelling unwanted invaders such as viruses and toxins that threaten its health, and managing its myriad everyday tasks in the face of unceasing thermally induced noise. Industry sectors such as

chemicals processing, personal care products, and pharmaceutical companies also need to know how their products interact on a molecular scale so that they can learn how to make them more effective, with less waste, and more cheaply. The drive to understand how molecular details propagate to the macroscopic scale in soft materials (Lipowsky *et al* 2005) therefore spans industry, academic research centres and government (ChemicalIndustryVision 2020), and demands increasingly complex and expensive experiments.

Visualizing the motion within complex fluids and soft materials yields valuable insight into how they respond to modification of their molecular constituents, but unfortunately much of the important behaviour is invisible to direct observation as the structures involved are smaller than the wavelengths of visible light. Electron microscopy allows one to see details 1000 times smaller, but only provides static snapshots of what are, in reality, ever-changing systems. There is therefore a need for techniques that can reveal what molecules and fluids are doing between 1 and 1000 nm on timescales from 1 ns to 1 ms: the *mesoscale* realm (Lipowsky 2004).

Membranes are ubiquitous in nature, and are essential for cellular life. Many crucial biological functions from structural support, through the ingestion, distribution and discharge of materials, to signal transduction and inter-cellular communication, take place at or near membranes. In the 30 years since it was realized that the cellular plasma membrane is a *fluid* bilayer (Singer and Nicholson 1972) our knowledge of membranes has increased enormously. This progress has relied on both experimental results and theoretical ideas. It is now routine to construct and characterize artificial membrane-bounded bubbles (or *vesicles*) with sizes from a few tens of nanometres up to tens of microns out of natural or modified phospholipid molecules (Rosoff 1996). Such vesicles are increasingly important in biotechnological applications (Torchilin 2005), although non-biological amphiphiles, such as diblock copolymers, also form vesicles (Discher and Eisenberg 2002) that have more widely tunable material properties making them more promising for applications such as drug delivery vehicles (Meng *et al* 2005). On the theoretical side, continuum theories based on bending elasticities (Canham 1970, Helfrich 1973, Evans 1974), in which the membrane is treated as an infinitely thin elastic sheet, continue to provide insight into many processes (Lipowsky and Sackmann 1995), but lack molecular detail. No theory can yield complete information on the behaviour of biological membranes, and this has led to the development of a variety of computational models that try to capture only those details that are relevant for the processes of interest. These models help in developing a greater understanding of the dynamic role of membranes in biophysical and biochemical processes in the cell, and their rational design for biomedical applications.

The remainder of this review is organized as follow. In the next section, we survey the simulation techniques that have been developed for the study of simplified models of biological membranes, particularly those applicable to vesicle fusion. Dissipative particle dynamics is a method that is being increasingly used for the study of soft materials. We provide an introduction to the history and principles of the DPD technique. Section 3 presents our results. Mesoscale simulation methods typically have numerous parameters whose values must be input into the technique. We show how atomistic molecular dynamics (MD) simulations may be used to calibrate the parameters of a DPD model of a diblock copolymer membrane allowing the DPD model to be applied to much larger systems (Ortiz *et al* 2005). Next, we summarize recent work (Shillcock and Lipowsky 2005) in which an initial global tension in their membranes promotes fusion of a vesicle to an adjacent planar membrane, and show that the process is stochastic and unreliable due to the appearance at high tension of alternative outcomes that compete to reduce the tension. New results are then presented which indicate how local forces applied to (a simplified model of) rigid proteins embedded in the membranes of a tensionless vesicle and adjacent, tensionless planar membrane can reliably and reproducibly drive them to fuse, as illustrated in figure 1. In section 4, we discuss the progress made in applying

mesoscale simulation methods on the length- and timescales of cellular processes, and conclude by suggesting a route for their future development to even larger length- and timescales.

2. The computational route to membrane fusion

In the last 15 years, mesoscale or *coarse-grained* computer simulations have emerged as an important tool for studying the assembly and properties of amphiphilic membranes. It is possible to construct near-molecular resolution models of vesicle fusion in which tens of thousands of amphiphiles interact on a 100 nm length-scale for several microseconds, as described in section 3.3 and in Shillcock and Lipowsky (2005), and to follow (somewhat smaller) fusion events for hundreds of microseconds (Stevens *et al* 2003). Coarse-grained simulation techniques reach these length- and timescales by a combination of collecting groups of atoms, or molecular groups, into particles or beads, providing a spatial coarse-graining; and replacing the complex atomistic force fields, which typically involve Lennard-Jones potentials, with softer effective forces, allowing a temporal coarse-graining. Because the soft forces allow a larger integration time step in solving the Newtonian equations of motion, coarse-grained simulation techniques are being extensively developed for studying biological systems, including membranes and protein-driven biophysical processes, whose natural length- and timescales exceed those that are achievable using more traditional atomistic molecular dynamics simulations.

A consequence of the coarse-graining is that effective parameters appear whose values are not directly connected to the molecular-scale interactions, and must be input into the technique. However, the almost unlimited control over these parameters contrasts with experiments where many parameters are poorly controlled or inextricably coupled. Such control allows the consequences of rational modification of molecular details on large-scale material properties to be systematically explored. For many applications it may be preferable to obtain semi-quantitative results for a large range of molecular parameters rather than more accurate results for a restricted region of parameter space. These results can then be used to focus computational resources on a more restricted problem space, thereby reducing the time and cost required to engineer materials with desired behaviour, or to follow biophysical processes over large length- and timescales.

Fluid membranes have also been studied by Monte Carlo simulations of geometric membrane models which are governed by the bending elasticity of the membranes. In this way, both the adhesion of oriented membrane segments (Lipowsky and Zielinska 1989, Rozycki *et al* 2006) and the behaviour of closed vesicles (Gompper and Kroll 1997, Kumar *et al* 2001) have been studied. In the present article, we focus on molecular models for bilayer membranes and emphasize recent simulation studies of membrane fusion.

2.1. Self-assembly and dynamical properties of amphiphilic membranes

Early attempts at modelling aggregates of amphiphilic molecules focused on the simpler (in a computational rather than physical sense) processes of self-assembly and equilibrium properties. Surfactant micelle self-assembly using coarse-grained MD simulations was first presented in 1990 (Smit *et al* 1990), and later models explored the dependence of micelle properties on surfactant architecture (Palmer and Liu 1996). These models were limited to small systems, containing of the order of tens of amphiphiles, because of the limitations of the available computer hardware. The subsequent increase in computer processing speeds allowed similar micellar systems and planar lipid bilayers to be simulated within a few years using atomistic MD (Marrink *et al* 2000, Tieleman *et al* 2000, Marrink *et al* 2001, Hofsäss *et al* 2003, Hyvönen and Kovanen 2003, Falck *et al* 2004). During this time, coarse-grained

simulation methods were developed to allow systems to be followed for longer times than was possible using traditional all-atom MD. Self-assembly and measurement of the equilibrium properties of planar lipid bilayers, including the lateral stress profile and surface tension, using a coarse-grained MD model was first performed in 1998 (Goetz and Lipowsky 1998), and this work introduced additional degrees of freedom into the coarse-grained lipid model such as the bending stiffness of the hydrocarbon chains. Soon after, the same lipid bilayer model was explored using DPD (Venturoli and Smit 1999). A variety of coarse-grained MD models have since been used to measure the equilibrium properties of planar lipid membranes containing a few hundred lipids (Goetz *et al* 1999, Shelley *et al* 2001), and such schemes have also been used to simulate vesicle fusion as will be discussed in section 2.2.2. Vesicle formation has been simulated using DPD (Yamamoto *et al* 2002), coarse-grained MD (Marrink and Mark 2003a) and atomistic MD (De Vries *et al* 2004). However, the huge computational resources needed to simulate a complete vesicle has stimulated the development of alternative techniques.

One approach to increasing the system size achievable by coarse-grained models is to eliminate the solvent particles. Because this eliminates the hydrophobic effect that drives the formation of amphiphilic membranes, solvent-free models are obliged to include more complex inter-molecular forces to restore its effects. One 'water-free' model of a fluid membrane (Farago 2003) uses non-additive, pairwise potentials between amphiphiles to cause them to assemble into, and remain in, a planar bilayer structure. The amphiphiles in this model are rigid rods containing a single hydrophilic head particle and two hydrophobic tail particles connected in a linear chain. The model possesses both fluid and crystalline phases as the area per molecule is varied, and allows the extraction of the membrane's elastic properties. Pores are found to form in the membrane at low area densities that promote inter-monolayer flip-flop of molecules. The importance of pore formation to the process of vesicle fusion is supported by their appearance in Monte Carlo (MC) simulations of the process (Müller *et al* 2003) described in section 2.2.3.

Pore formation in membranes is usually viewed as an extension of classical nucleation theory (Litster 1975), and is therefore treated as an activated process that depends on the competition between a stretching force (or surface tension) that tries to increase the pore area, and an energy cost per unit length of pore edge (or edge tension) that tries to minimize the pore boundary. The shape of the pore is most often taken to be circular (Litster 1975, Tolpekina *et al* 2004). This assumption is correct at zero temperature, when energy terms dominate the pore's behaviour, but may be incorrect at finite temperature or for membranes with impurities that sufficiently lower the energy cost for pore formation and expansion. Pore formation in membranes at finite temperature has been studied using lattice-based MC (Fournier and Joos 2003), off-lattice MC (Shillcock and Seifert 1998), field theoretic methods (Sens and Safran 1998), and atomistic MD simulations (Tieleman *et al* 2003). In the second of these studies, the entropy of shape fluctuations of the pore rim and the appearance of multiple pores are both enhanced at finite temperature, and render the membrane unstable to rupture even at zero lateral tension. In the third study, out-of-plane fluctuations of circular pores are predicted to retard pore formation. The MD simulations of Tieleman *et al* (2003) reveal differences in the molecular transformation that takes place when a lipid membrane is placed under mechanical or electrocompressive stress. Mechanical stress causes significant membrane thinning followed by the appearance, and rapid growth, of a cylindrical pore lined with lipid headgroups, whereas an electric field tends to produce a pore in which the water molecules are highly oriented. Pore formation driven by nonionic surfactants interacting with lipid membranes has been simulated using DPD (Groot and Rabone 2001). Recently, a statistical mechanical model for pore formation in fluctuating membranes has been developed (Farago 2005) that predicts that a weakly stretched membrane can be unstable to thermally induced

pores. Both the membrane surface tension and the pore edge tension are renormalized at sufficiently high temperatures by the fluctuations of the membrane and pore shape, so that a finite-sized pore can be entropically stabilized. This entropy-induced instability is consistent with MC simulations of pore formation in two-dimensional membranes (Shillcock and Seifert 1998).

Brownian dynamics (BD) simulations have been used to follow the self-assembly of amphiphilic bilayer vesicles containing around 1000 molecules and no explicit solvent (Noguchi and Takasu 2001a). The amphiphiles are again represented by rigid rods containing one hydrophilic head particle and two hydrophobic tail particles. The absence of solvent is compensated by complex non-local interactions between the amphiphiles. In these BD simulations, once the forces have been specified between interacting particles, a set of underdamped Langevin equations is solved to generate the positions of the particles. Random forces are added independently to each particle's equation of motion to represent the effects of thermal noise in the system. The dynamics of the systems is therefore diffusive. Application of this model to vesicle fusion is described in section 2.2.3.

Another example of a solvent-free model is embodied in the Espresso code (http://www.espresso.mpg.de). This has been used to study the self-assembly and material properties of amphiphilic membranes (Cooke *et al* 2005). An amphiphile in this work is a three-particle, linear chain containing one hydrophilic head particle and two hydrophobic tail particles. The chains are flexible, however, and possess a long-range attractive potential between their tail particles that serves to drive self-assembly of the molecules into a membrane aggregate. The range of this attractive potential is a key parameter, and can be used to tune the membrane's elastic properties. Realistic values of $5–20k_BT$ are found that make the model suitable for lipid membrane simulations. This makes the scheme very attractive for studies of membrane processes such as domain formation in multi-component membranes, budding in vesicles, and dynamic processes such as the engulfment of a colloidal particle by a membrane. As an example of its applications, figure 2 shows the formation of domains and a bud in a 60 nm diameter, two-component vesicle, which contains about 16 000 molecules. Domain formation is driven by the preference of the two types of amphiphile to pack next to their own kind instead of mixing. Such buds are also seen in off-lattice Monte Carlo simulations of two-component vesicles (Kumar *et al* 2001), which are also able to probe long length-scales and follow the formation and evolution of dozens of buds on a vesicle's surface.

A final example of a solvent-free model has been introduced recently (Wang and Frenkel 2005). An amphiphile is again represented by a three-bead linear molecule containing a single hydrophilic bead and two hydrophobic beads. The beads are connected by finitely extensible nonlinear elastic (FENE) springs, and the molecule is not rigid but possesses a bending stiffness potential. The absence of the solvent is compensated for using a multibody density-dependent potential similar to that of the Noguchi model (Noguchi and Takasu 2001a), although the details differ. Off-lattice Monte Carlo simulations are used to generate the states of the system, and ensemble averages provide the mean values of equilibrium observables. The model produces lateral diffusion coefficients and elastic moduli in good agreement with experimental data on typical lipid vesicles (Rawicz *et al* 2000).

Although solvent-free models gain a computational advantage through not using processor cycles to simulate the bulk solvent, their continued development for studying vesicle fusion is probably limited. As current fusion models advance so as to include diffusing species such as signalling molecules, the hydrodynamic flow of a vesicle's internal solvent being expelled under pressure, and, eventually, many vesicles held near the pre-synaptic plasma membrane in a more realistic model of synaptic vesicle fusion, the absence of solvent will be a disadvantage. Secondly, while providing an excellent framework for studying equilibrium properties of

membranes, their dynamics do not correspond to the Newtonian equations of motion. We note here that while explicit solvent schemes, such as DPD, improve on the solvent-free techniques in that they incorporate hydrodynamic forces, it is still non-trivial to capture all the dynamic properties of a fluid. As an example, the transport of momentum in a bulk DPD fluid occurs on the same timescale as the particle motion, resulting in the fluid's Schmidt number being smaller than that of the real fluid (Groot and Warren 1997). However, recent improvements to the DPD method (Stoyanov and Groot 2005) have removed this restriction, and demonstrated that DPD can be used to simulate fluids in which momentum transport and particle transport are governed by well separated timescales.

2.2. Vesicle fusion

Vesicle fusion is essential for cell viability, and takes place in processes as diverse as signal transmission at neuronal synapses, fertilization of an egg by a sperm, and viral entry into cells. This appears to conflict with the primary requirement of biological membranes, which is to provide a barrier between intracellular compartments, and between a cell and its external environment. Understanding how the stability of lipid membranes is overcome by the cellular protein machinery when required is a major topic of research, and several reviews have appeared in the last few years (Mayer 2001, 2002, Jahn and Grubmüller 2002, Jahn *et al* 2003, Tamm *et al* 2003), including two recent ones (Ungermann and Langosch 2005, Chernomordik and Kozlov 2005). Although fusion of giant (1–20 μm diameter) vesicles can be observed using fluorescence microscopy (Lei and MacDonald 2003), optical dark-field microscopy (Nomura *et al* 2004) and fast optical microscopy with a temporal resolution of 50 ms (Haluska *et al* 2006); and SNARE-mediated fusion of liposomes to a supported planar membrane has been followed using total internal reflection fluorescence microscopy (Fix *et al* 2005), the molecular rearrangements that take place during the final stage of the fusion process, where the two initially distinct membranes join and produce a fusion pore, cannot yet be resolved by these experimental techniques.

Continuum elastic theories of membrane deformations have proposed possible static intermediate structures, such as hemifusion, in the fusion process; and there is recent experimental evidence supporting these theories (White and Castle 2005, Xu *et al* 2005). However, unexpected results not contained in these theories have appeared in membrane fusion simulations (Müller *et al* 2003, Katsov *et al* 2005) that also have experimental support (Shangguan *et al* 1996, Bonnafous and Stegmann 2000, Frolov *et al* 2003). This suggests that there is still some way to go before membrane fusion can be said to be understood. The continued application of the computational methods discussed in this review should aid in illuminating on a molecular scale the stages of the fusion process.

2.2.1. Local membrane contacts and stalks: continuum models. The idea that membrane fusion is preceded by a *local* contact between the two membranes arose in the 1970s and led to the first proposals about transient states with point-like defects, so-called stalks, in which the proximal monolayers of the two bilayers are connected whereas the two distal monolayers are still separated (Gingell and Ginsberg 1978, Hui *et al* 1981). In a series of theoretical papers, a variety of specific stalk structures have been proposed and their energies estimated using continuum models based on the bending elasticity of the membranes (Kozlov and Markin 1983, Markin *et al* 1984, Siegel 1993, 1999, Kuzmin *et al* 2001, Markin and Albanesi 2002, Kozlovsky and Kozlov 2002). These different continuum models for stalks have been reviewed by Lentz *et al* (2002) and by Tamm *et al* (2003).

One assumption that is implicitly made in most of these stalk models is that the stalk energy corresponds to the energy barrier for the fusion process. However, this assumption is
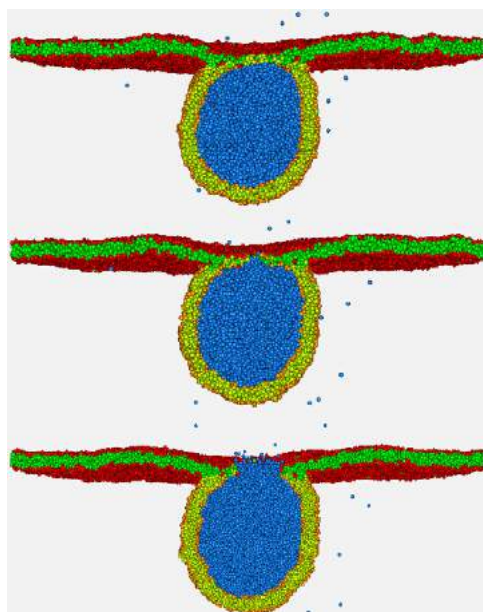
Figure 1. High-resolution visualization of the molecular rearrangements that take place as a tense 28 nm diameter vesicle fuses to a tense 100×100 nm^2 planar membrane. The fusion event is simulated using explicit-solvent dissipative particle dynamics in a 100 nm $\times$ 100 nm $\times$ 42 nm simulation box containing over 3 000 000 particles. The vesicle is composed of 5887 lipids and the planar membrane contains 28 000 lipids of the same type. For further details of the fusion protocol see section 3.2 in the text. The images are taken 192 ns (top), 240 ns (middle) and 256 ns (bottom) after first contact of the two membranes. The top image shows the contact zone just before the fusion pore appears and indicates that many vesicle lipids (orange heads and yellow tails) have translocated into the planar membrane's *cis* leaflet, displacing those originally from the planar membrane (red heads and green tails), but fewer than six have flip-flopped into the planar membrane's *trans* leaflet as determined from visual inspection. The middle image shows the fusion pore when it has a diameter of a few lipid headgroups and the vesicle's internal solvent particles have just started to emerge. The bottom image shows the fusion pore when it has grown to approximately the radius of the vesicle. Note that the vesicle's internal solvent has not emerged very far in this short time (approximately one membrane width, or 4 nm), and that subsequent diffusion of the solvent particles may be significantly slower than the fusion event time of 320 ns that is defined as the time from first membrane contact until the pore has expanded to the diameter of the vesicle. (Images created using TGS Amira visualization software, mercury computer systems: www.tgs.com.)

not at all obvious. First, the bilayer states considered in these continuum models have rather smooth lipid–water interfaces. By contrast, all computer simulations of bilayer membranes with molecular resolution show that these interfaces are roughened by thermally excited displacements or protrusions of individual molecules. Second, all stalk states considered in the continuum theories are highly symmetric. Indeed, they are taken to be both axi-symmetric and up–down symmetric. It seems rather unlikely that real bilayers will attain a *transient* state with such a high symmetry. Third, two adhering bilayers are separated by a water layer with a thickness of 1–2 nm. Part of this water is believed to be bound to the lipid head groups. In order to establish a local point-like contact between the two proximal monolayers of the two bilayers, this bound water has to be pushed to the side. In fact, Kuzmin *et al* (2001) used a continuum model to estimate the work of dehydration that enters the energy barrier between a nipple state—corresponding to two bilayers that are smoothly bent towards each other—and a stalk state. The most likely candidate for such a barrier is provided by bilayers that are rather
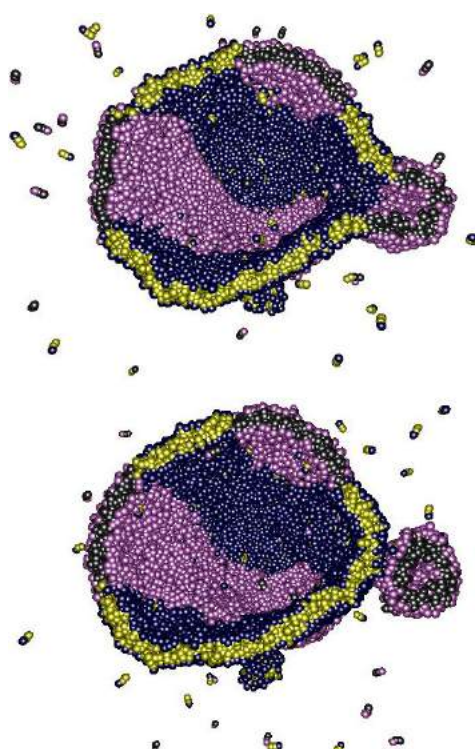
Figure 2. Illustration of domains and a bud forming from a two-component vesicle containing 16 000 HT$_2$ lipids using the *ESPRESSO* solvent-free molecular dynamics code (http://www. espresso.mpg.de). The vesicle contains a 50:50 mixture of two lipid types, A (black heads and yellow tails) and B (violet heads and black tails). The Lennard-Jones (LJ) interaction ranges are $w_{AA} = w_{BB} = 1.5\sigma$, $w_{AB} = 1.3\sigma$ in the notation of Cooke *et al* (2005). These values lead to phase separation in the membrane as the attractive pieces of the LJ potentials satisfy AB < AA = BB. The diameter of the vesicle prior to phase separation is 60 nm, and the phase separation takes place over a time of approximately 60 μs. The bending stiffness of the pure vesicle membrane (both A type and B type) is estimated to be 8 kT. The first snapshot shows a bud developing that still has its internal volume continuous with the vesicle's interior. The second snapshot shows the bud when it has sealed off, separating its interior volume from that of the vesicle. Also visible is a small protrusion at the bottom of the larger vesicle. Lipids that have left the vesicle membrane are visible floating freely in the exterior volume. These lipids are in equilibrium with those in the vesicle. (Images provided by Ira Cooke and Markus Deserno with permission.)

disordered by molecular protrusions. The latter state will look rather different from the ordered and highly symmetric stalk conformations considered in the continuum theories.

Therefore, it seems likely that the energy barrier for fusion is provided by a disordered and partially dehydrated state. In principle, the latter state could subsequently transform into a stalk-like state that is located on the 'downhill slope' of the fusion pathway (such an assumption seems to be behind the calculation of Kuzmin *et al* (2001)). However, if the stalk-like state does not represent the barrier and, thus, does not correspond to a saddle point in the high-dimensional energy landscape, it competes with many other states on the 'downhill slope', and there is no obvious reason why the fusion pathway should pass through such a stalk at all.

The restrictions of the continuum theories to a small subset of highly symmetric stalk states can be overcome by particle-based simulations that allow the exploration of the whole conformational space of the two bilayers. One of these possible conformations is a hemifused

state. Recent experiments have found evidence that hemifusion is an intermediate state in the fusion of liposomes containing recombinant SNARE complexes (Lu *et al* 2005) and *in vitro* viral fusion to cells (Melikyan *et al* 2005). In addition, one should also note that all continuum models for the various stalk conformations addressed essentially *tensionless* membranes. *A priori*, such a model seems to be consistent as long as the tension σ and the bending rigidity κ lead to a crossover scale $(\kappa/\sigma)^{1/2}$ that is large compared to the adhering membrane segments. However, our recent simulations have shown that membrane tension represents an important control parameter for the fusion process and acts to *increase* the fusion probability; see further below.

2.2.2. Molecular dynamics simulations of vesicle fusion. Current *in vitro* vesicle fusion assays indicate a timescale of tens of milliseconds for fusion (Kiessling 2005, Liu *et al* 2005), and *in vivo* experiments suggest it may require hundreds of microseconds (Lindau and de Toledo 2003). The relevant length-scales range from less than a nanometre for the initial fusion pore width up to tens of microns for the vesicle diameter. This renders the use of atomistic MD simulations computationally prohibitive, and even coarse-grained MD simulations are restricted to small systems. Atomistic MD simulations are being used to address spatially restricted questions of importance to fusion, such as phase transitions between different lipid phases (Marrink and Tieleman 2002), and whether the headgroups of lipids in closely apposed membranes dehydrate sufficiently so as to initiate fusion (Ohta-lino *et al* 2001). The latter work showed that dramatic redistributions of lipids do occur under dehydration conditions, but the membranes were restricted to 56 lipid molecules each. A recent review of the role of lipids in initiating membrane fusion (Kinnunen and Holopainen 2000) discussed the existence of an 'extended' conformation in which the two tails of some lipid molecules rearrange so as to span the two apposed membranes. The authors point out that such conformations are not prohibited by physical or chemical factors, and evidence for their existence has been found in fluorescence spectroscopy experiments (Holopainen *et al* 1999). Their appearance in atomistic MD simulations suggests that further exploration and visualization of the molecular rearrangements that take place at the onset of fusion are important.

The atomistic MD technique uses atoms as its fundamental constituents with complex potentials tuned to reproduce the structural properties of relevant systems of interest. Once the molecules and their interactions are specified, the algorithm integrates Newton's equations of motion to generate the system's dynamical behaviour, which should apply as long as the size of the particles is large compared to their de Broglie wavelength. The great advantage of MD simulations is that the dynamics of the system are (presumably) the same as those obeyed by the physical system, and the maximum information is gained about all processes taking place within the length- and timescales of the simulation. The same advantages are present in coarse-grained MD simulations, except that some ambiguity is introduced in assigning mass-, length- and timescales due to the use of effective potentials. However, this cost is outweighed by the enormous increase in system size, from tens of lipid molecules in atomistic MD to thousands in coarse-grained MD simulations. For this reason, almost all MD studies of fusion use some degree of coarse-graining of the molecules.

Coarse-grained MD simulations of the fusion of two 15 nm vesicles, containing about 1000 lipids each, found that constraining the vesicles to be close together for tens of nanoseconds was sufficient to cause them to fuse (Marrink and Mark 2003b). Successful fusion depended on the lipid species in the vesicles: mixtures of dipalmitoylphosphatidylcholine (DPPC) and palmitoyl-oleoyl phosphatidylethanolamine (POPE) fused most easily at separations up 1.5 nm; vesicles composed of pure DPPC only fused when held together closer than 1 nm for more than 50 ns; and vesicles containing DPPC and 25% lysoPC were not seen to fuse at all within

200 ns. The initial contact between the vesicles was provided by a few lipids whose protrusion fluctuations caused them to merge into the apposed monolayer. The small size of the vesicles, and consequent high curvature, provides a strong driving force for the observed fusion.

The fusion pathway observed in these simulations proceeds as follows. First, a contact zone, or stalk is formed by the *cis* monolayers. Next, the stalk converts into a transmembrane contact in which the *trans* monolayers touch. Finally, the contact zone ruptures and the inner compartments of the vesicles become contiguous. An unexpected finding in some of the fusion events was the mixing of lipids from both the outer and inner monolayers. This appears to result from a reduced line tension for pore formation in the vicinity of the stalk, and an asymmetrical expansion of the contact zone into a 'banana-shaped' region.

Similar results have been obtained by Stevens *et al* (2003), who simulated the fusion of two vesicles containing about 1000 lipids each for hundreds of microseconds. In this protocol, a transient force was applied to all membrane molecules in the vesicles to push them together. The force was removed after a few lipids had exchanged between the vesicles. In these simulations, fusion appeared to start at the edge of the flattened contact zone between the two vesicles, where the curvature of the surface is greatest. Interestingly, this results in the fusion pore forming at points quite distant from the point of closest approach of the vesicles. Similar to the work of Marrink and Mark (2003b) just described, the stalk in these fusion events appears to expand asymmetrically around the strained edge of the contact zone, leading to a partially confined solvent cavity between the two liposomes.

2.2.3. Alternative fusion models. The computational cost of even coarse-grained MD simulations of vesicle fusion currently restricts their application to small systems, such as the 15 nm diameter vesicles described above. Progress towards larger length- and timescales is currently only possible using still more coarse-grained approaches.

Canonical ensemble, lattice Monte Carlo simulations in three dimensions have recently been used (Müller *et al* 2003) to explore the fusion of two closely apposed, tense planar membrane patches composed of copolymers with a hydrophilic head part and a hydrophobic tail part. The size ratio of the hydrophilic to hydrophobic sections (11 segments and 21 segments respectively) is chosen to be close to that appropriate to biological lipids. The solvent is a homopolymer. The relative sizes of the copolymer and solvent polymer and their mutual repulsion are chosen so as to ensure that there is a well defined separation between the hydrophilic and hydrophobic regions of the membrane and that it is larger than the lattice spacing. The molecules in these simulations do not obey Newtonian dynamics, but evolve according to a Markov process (using the Metropolis algorithm) that ensures the correct statistical weight for states of the system in equilibrium. Ensemble averages then provide the connection with physical properties. Because the total densities of each segment type are conserved, the motion of the polymers is diffusive. The bond fluctuation model is employed that allows the MC parameters to be mapped onto the standard Gaussian chain model of polymeric mixtures. The membranes are placed under an initial tension by specifying the number of molecules in them so as to set the area per molecule greater than its preferred value. The initial solvent-filled gap between the membranes has a width approximately equal to one half of the bilayer thickness.

Contacts between the molecules in the membranes arise naturally in this model as a result of thermal shape fluctuations. Most of these contacts rapidly disappear, but some lead to formation of a 'stalk' or merging of regions of the closest (*cis*) monolayers. Once a stalk has formed, the probability of a hole appearing in one or other bilayer near the stalk increases markedly. The presence of the nearby hole then appears to cause the stalk to traverse around it and form a ring-like connection between the membranes. The authors explain the increased

probability of hole formation close to a stalk as the result of a lowering of the line tension around such a hole caused by the reduction in the curvature of the piece of membrane between the hole and the stalk. The final stage in the observed fusion process is the appearance of a second hole in the other membrane and the movement of the stalk to surround both holes. This results in the full fusion pore connecting the distal sides of the membranes. Similar results have been observed in dynamic self-consistent field theory (SCFT) simulations on large systems of symmetric, amphiphilic diblock copolymers, including the observation of pore formation close to the stalk connecting two fusing membranes (Sevink and Zvelindovsky 2005). Recent work on a similar model using SCFT methods emphasizes the key role of the line tension in this interpretation of membrane fusion (Katsov *et al* 2005). The authors conclude that as fusion is an activated process, and the line tension opposing the growth of a pore in the membrane appears quadratically in the Boltzmann factor, any local perturbation in the membrane (such as that provided by the presence of the stalk near the pore) that reduces the line tension can hugely increase the probability of the pore growing and the fusion process completing (Schick *et al* 2005).

Other simulation studies of vesicle fusion have used rigid, amphiphilic rods to represent the lipids and removed the solvent entirely. Chanturiya *et al* (2002) used a two-dimensional model of 'ring-like' vesicles and varied the tension in the bilayers and the internal 'pressure.' They found that hemifusion could be induced by increasing the lateral tension in one of the bilayers, and full fusion of two vesicles occurred if an internal over-pressure was introduced. If the pressure was increased too much, the vesicles ruptured in more than one place, including points distant from the contact zone.

Brownian dynamics simulations of three-dimensional vesicle fusion have been performed (Noguchi and Takasu 2001b) using the technique previously applied to vesicle self-assembly (Noguchi and Takasu 2001a). Each vesicle contained about 1000 rigid rod-like amphiphiles composed of one hydrophilic head bead attached to two hydrophobic tail beads. The vesicles were approximately 20 nm in diameter. Fusion of the vesicles was observed at different temperatures, and a stalk intermediate was observed whose behaviour varied with the temperature of the system. Fusion events at the lower temperature followed a sequence in which the outer leaflets merge first, followed by the formation of a trans-membrane contact that expands until the fusion pore appears. The system at the higher temperature follows a different pathway to fusion that is similar to that observed in the MC simulations of Müller *et al* (2003). Once the stalk forms it does not expand in a radially symmetric way but, if a pore forms in one of the bilayers nearby, it deforms into an ellipse that traverses around the pore taking up a ring-like structure. If a second pore forms in the other bilayer, both pores merge into a full fusion pore. The appearance of a similar process in two quite different simulation techniques suggest that it is robust against details of the methods, and may be relevant to physical processes that occur during vesicle fusion.

The models of vesicle fusion described so far contain a few hundred amphiphiles in membrane patches or vesicles of linear dimension 10–15 nm. In section 3, we present results on the fusion of 28 nm diameter vesicles to planar membrane patches of up to $100 \times 100 \text{ nm}^2$ containing approximately 6000 and 28 000 amphiphiles respectively. But first we introduce the DPD method and show how it can be used to study the material properties and behaviour of membranes and vesicles.

2.3. Dissipative particle dynamics method and implementation

In this sub-section we provide a brief history of the dissipative particle dynamics (DPD) simulation method, and then describe the implementation that we have used to generate the results of section 3.

2.3.1. A short history of the DPD method.   Dissipative particle dynamics was invented in 1992 by Hoogerbrugge and Koelman (1992) in an attempt to go beyond the limitations of atomistic MD simulations, whilst retaining some molecular detail including the hydrodynamic interactions. Subsequent modifications to the original algorithm (Espagnol and Warren 1995, Groot and Warren 1997) ensured that the equilibrium states of the system are Boltzmann distributed, and established the Groot–Warren integrator as the most common algorithm used by subsequent workers. An early review of the technique was published by Warren (1998), and a comparison of various methods of simulating surfactant solutions followed soon after (Shelley and Shelley 2000). A derivation of the DPD scheme from a set of underlying MD particles allows the simulation of dissipative particles whose size can change with time, improving the scheme's performance when multiple length scales appear in a simulation, such as for hard colloidal particles in a solvent (Flekkoy and Coveney 1999). Early applications of the DPD technique included microphase separation of polymeric mixtures (Groot and Madden 1998), the dynamics of an oil droplet near a hard surface in shear flow (Jones *et al* 1999), self-assembly of a planar membrane (Venturoli and Smit 1999), aggregation of surfactants onto a polymer in a bulk surfactant solution (Groot 2000), colloidal motion in a solvent (Whittle and Dickinson 2001), and rupture of a planar membrane patch by incorporation of nonionic surfactants (Groot and Rabone 2001). It was also applied to the evolution of the interface between pure surfactant and water (Prinsen *et al* 2003) and the behaviour of grafted polymer brushes subject to shear flow (Irfachsyad *et al* 2002).

A series of papers then appeared applying the method to the measurement of equilibrium properties of bilayer membranes. These included measurements of the lateral stress profile and the membrane surface tension (Shillcock and Lipowsky 2002), the dependence of a membrane's material properties on the symmetry and length of the tails of two-tailed amphiphiles (Illya *et al* 2005), the appearance of different phases of a membrane as the temperature and amphiphile interactions are varied (Kranenburg *et al* 2003), and the packing of surfactants at an oil–water interface and their efficiency at reducing the surface tension (Rekvig *et al* 2003). A novel extension of the method allows the inclusion of electrostatic forces between a polyelectrolyte and charged surfactants in bulk solution (Groot 2003), although to our knowledge this has not been used in other studies. Lately, DPD has been used to follow the budding and fission of two-component vesicles (Yamamoto and Hyodo 2003), the aggregation of copolymer analogues of the exon1 fragment of Huntington's disease proteins driven by the relative hydrophobicity of different regions of the fragment (Burke *et al* 2003), the tension-induced fusion of a vesicle to a planar membrane (Shillcock and Lipowsky 2005), the behaviour of a worm-like chain model of DNA polymers (Symeonidis *et al* 2005), and the influence of model proteins embedded in a fluid membrane (Venturoli *et al* 2005).

During this time, several extensions or modifications to the technique have been proposed. Some are attempts to improve the scheme's thermostat, which has been shown (Besold *et al* 2000, Nikunen *et al* 2003, Jakobsen *et al* 2005) to lead to spurious behaviour if too large a time step is used in the integration scheme. These include modifying the thermostat (Lowe 1999, Peters 2004), thereby improving the temperature control (Den Otter and Clarke 2001), and combining two different thermostats and randomly selecting one or the other for each interacting particle pair, that allows the viscosity of a DPD fluid to be varied by orders of magnitude (Stoyanov and Groot 2005). The latter thermostat can also be applied to other particle-based simulation techniques, such as MD (Soddemann *et al* 2003). Other changes have been suggested to allow simulations in new ensembles such as constant pressure and constant surface tension ensembles (Jakobsen 2005), and to replace the original potentials with density-dependent ones that include an attractive part, thereby allowing liquid–gas interfaces to appear in the simulations (Warren 2001), a process that is forbidden in the original algorithm by the

quadratic nature of the DPD fluid's equation of state. We now summarize the Hoogerbrugge–Koelmann/Groot–Warren scheme that we have used in generating the results in previous work (Shillcock and Lipowsky 2002, Ortiz *et al* 2005, Shillcock and Lipowsky 2005) and those presented in section 3.

2.3.2. Implementation of the DPD method. The elementary units in a DPD simulation are fluid elements or *beads*. A bead represents a volume of fluid that is large on a molecular scale, and hence contains at least several molecules, or molecular groups, but is still macroscopically small. Beads interact via effective forces chosen so as to reproduce the hydrodynamic behaviour of the fluid without reference to its molecular structure. DPD differs in this respect from MD simulations, in which the forces are chosen to model the inter-molecular interactions of a system as accurately as possible. Forces in DPD are pairwise additive, conserve momentum, have no hard core and are short ranged, the range of the force defining the size of the beads. The use of momentum-conserving forces also distinguishes DPD from Brownian dynamics, in which each particle receives an independent random push, resulting in purely diffusive motion.

The beads have the same mass, m_0, and diameter, a_0, and these set the mass- and length-scales in the simulation. A timescale must be extracted from the dynamics of relevant processes in the simulated system. Because we work with fluid membranes and vesicles, we use the in-plane amphiphile diffusion coefficient to set the timescale. This is obtained by calculating the average of the mean square displacement of all the molecules in a membrane, and taking the ratio of its long-time limiting value to the elapsed time as a measure of the diffusion coefficient.

Beads in a DPD simulation interact via three forces: a conservative force that gives each bead an identity and allows, for example, the representation of hydrophobicity between hydrocarbon and water; a random force that creates relative momentum between bead pairs; and a dissipative force that destroys relative momentum. Beads are considered to have (unobserved) internal degrees of freedom that give rise to the dissipative forces, and to be coupled to the local temperature of their (fluid) environment, that is the source of the random forces. The temperature parameter is determined by the ratio of the dissipative and random force coefficients, and is set to unity in our simulations. We use the form of the effective forces suggested by Groot and Warren (1997), who also showed that choosing the dissipative and random forces appropriately leads to equilibrium states of the system that satisfy the Boltzmann distribution.

The conservative force between two beads i, j separated by a distance r_{ij} is

$$F_{ij}^C = a_{ij}(1 - r_{ij}/a_0)\hat{r}_{ij} \tag{1}$$

for $r_{ij} < a_0$, and zero otherwise. The range of the force is set by a_0, and a_{ij} is the maximum force between beads of types i, j; r_{ij} is the distance between the centres of beads i, j, and $\hat{r}_{ij}$ is the unit vector pointing from bead j to bead i. Note that the conservative force is always finite, taking its maximum value, a_{ij}, at zero separation.

The dissipative force between two beads is linear in their relative momenta and takes the form

$$F_{ij}^D = -\gamma_{ij}(1 - r_{ij}/a_0)^2(\hat{r}_{ij}.v_{ij})\hat{r}_{ij} \tag{2}$$

where γ_{ij} is the strength of the dissipation between beads i, j, and $v_{ij} = v_i - v_j$ is their relative velocity (which is the same as their momentum as $m_0 = 1$ in our simulations).

Finally, the random force between a pair of beads is

$$F_{ij}^R = \sqrt{2\gamma_{ij}k_B T}(1 - r_{ij}/a_0)\zeta_{ij}\hat{r}_{ij} \tag{3}$$

where values of the random force are generated by sampling a uniformly distributed random variable, $\zeta_{ij}(t)$, that satisfies $\langle \zeta_{ij}(t) \rangle = 0$ and $\langle \zeta_{ij}(t)\zeta_{i'j'}(t') \rangle = (\delta_{ii'}\delta_{jj'} + \delta_{ij'}\delta_{ji'})\delta(t - t')$. The random force has the symmetry property $\zeta_{ij}(t) = \zeta_{ji}(t)$ that ensures local momentum conservation, and hence the correct hydrodynamic behaviour of the simulated fluid on long length-scales.

Molecules are constructed by tying beads together using Hookean springs with the potential

$$U_2(i, i+1) = \tfrac{1}{2}k_2(r_{ii+1} - l_0) \tag{4}$$

where $i, i + 1$ label adjacent beads in the molecule. The spring constant, k_2, and unstretched length, l_0, are chosen so as to fix the average bond length to a desired value. Both parameters may be specified independently for each bead type pair, allowing a molecule's bond strength to vary along its length.

Chain stiffness is modelled by a three-body potential acting between adjacent bead triples in a chain,

$$U_3(i - 1, i, i + 1) = k_3(1 - \cos(\phi - \phi_0)) \tag{5}$$

where the angle ϕ is defined by the scalar product of the two bonds connecting the pairs of adjacent beads $i - 1, i$ and $i, i + 1$. In general, the bending constant, k_3, and preferred angle, ϕ_0, may be specified independently for different bead type triples, allowing the chain stiffness to vary along a molecule's length. Typically, we use a preferred angle of zero so that the potential minimum occurs for parallel bonds in a chain.

Biological lipid molecules often possess two hydrocarbon tails, and have headgroups of different degrees of bulkiness. A simple architecture that reflects these properties, and which we use for all of the amphiphiles in our fusion protocols, consists of three hydrophilic beads (designated H) to which are attached two linear hydrophobic tails each containing four chain beads (C). Such an amphiphile is represented, using an obvious symbolism, as $H_3(C_4)_2$. The amphiphiles are contained within bulk solvent (W). Each solvent bead represents a small volume of bulk water consisting of several molecules. Because a solvent bead represents several molecules of solvent, and has a length-scale of the order of 1 nm, there is no explicit modelling of hydrogen bonds.

3. Results

In this section, we present recent results from DPD simulations of the fusion of vesicles to planar membrane patches. Different protocols are introduced for driving the fusion process, and a comparison of the simulation mechanisms with known results for *in vitro* fusion assays is made. The results have been generated using amphiphiles that are modelled on phospholipids, but are generally applicable to any amphiphilic species that form membranes. In particular, it would be very useful to study the fusion of non-phospholipid aggregates, such as vesicles composed of diblock copolymers, to explore the generality of the stages of the fusion process. As a first step in this process, we have constructed planar membrane patches and a complete vesicle out of an experimentally relevant copolymer and simulated its properties using DPD. These simulations show that modifications to the commonly used mapping of a constant mass for each coarse-grained bead in the DPD scheme are necessary in order to bring the material properties of the membranes into agreement with experimental data.

3.1. Calibrating a DPD polymersome using atomistic molecular dynamics

Whereas biological membranes are composed of lipid molecules with a fairly restricted architecture, membranes made of non-biological diblock copolymers are also of great interest

(Antonietti and Förster 2003). Because the architectural space of possible diblock copolymers is larger than that of lipids, vesicles composed of these molecules, which are also called *polymersomes*, have certain physical properties, such as the membrane thickness and critical area stretch before rupture, that span a wider range of values than lipid vesicles (Meng *et al* 2005). The interior structure of the membrane of a polymersome differs substantially from that of a phospholipid membrane. The hydrophobic block is sequestered between the well hydrated hydrophilic blocks, and the aqueous solvent penetrates to the edge of the hydrophobic region. The entanglement of the individual molecules leads to much slower in-plane diffusion, and a greater resistance to rupture under lateral stress. Recent experiments have explored the interactions of short, amphipathic peptides, such as alamethicin, with (uncharged) diblock copolymer membranes (Vijayan *et al* 2005) and found that even though the peptides are less than one half of the diblock membrane width they permeabilize it quite effectively. Other experiments using 50 μm diameter polymer vesicles have shown that they undergo fusion when subject to ultrasound (Zhou and Yan 2005), which makes them attractive as drug delivery vehicles. Molecularly detailed simulations of the fusion of polymersomes would be useful for exploring the molecular architectural space and the resulting variations in the fusion process. The results of such simulations would be relevant for both a fundamental understanding of polymersomes and their clinical applications.

Unfortunately, the high molecular weight of some diblock copolymers, and the large diameter of polymersomes, currently restricts atomistic MD simulations to a few tens of molecules, and even coarse-grained MD is limited to patches of a hundred or so molecules (Srinivas *et al* 2004a). These limitations, and the soft nature of polymer vesicles, makes them a prime target for DPD modelling. The variation in polymersome physical properties with the molecular weight of the constituent molecules forms an important link between experimental results, analytical theories and simulations. Ortiz *et al* (2005) have performed DPD simulations of membrane patches of diblock copolymers of various molecular weights, calibrating the DPD parameters using data obtained from atomistic MD simulations of the same system.

Typically, every bead of each molecular species in a multi-component DPD simulation is considered to contain the same amount of matter, and the self-interaction parameters are chosen so that the compressibility of each pure species matches that of water at room temperature. The cross-terms are then matched to the relative solubility of each species in the others. For species that are mutually soluble, such as the PEO block and water relevant for polymersome simulations, a different property has to be chosen. Ortiz *et al* (2005) choose the radial distribution function of PEO in water for this purpose. Using the conventional DPD mapping for simulations of a planar membrane patch of diblocks, they find that the geometry of the hydrophobic block is incorrect and the hydrophobic density is too high. This leads to unphysical values for the membrane area stretch modulus. A revised mapping was developed in which the beads of each species are considered to contain an amount of matter that depends on the species, and is chosen so as to reproduce the experimental bulk density. For the PEO–PEE diblock considered this led to the density-based mapping of 1.392 PEO monomers/bead, 0.774 PEE monomer/bead and 3.01 water molecules/bead. This is in contrast to the conventional mapping, in which all ratios are unity.

Using the new mapping, the membrane area stretch modulus is found to be 137 mN m^{-1}, which is in good agreement with the experimental value of 120 ± 20 mN m^{-1} (Discher *et al* 1999). Additionally, the scaling of the membrane hydrophobic block thickness with polymer molecular weight was found to obey the experimentally observed scaling law $d \sim M^{1/2}$. Neither of these results were obtained using the conventional DPD mapping. Figure 3 shows an example taken from Ortiz *et al* (2005) of the new MD/DPD mapping being used to calibrate a DPD simulation of the rupture of a polymersome. A 28 nm diameter polymersome containing
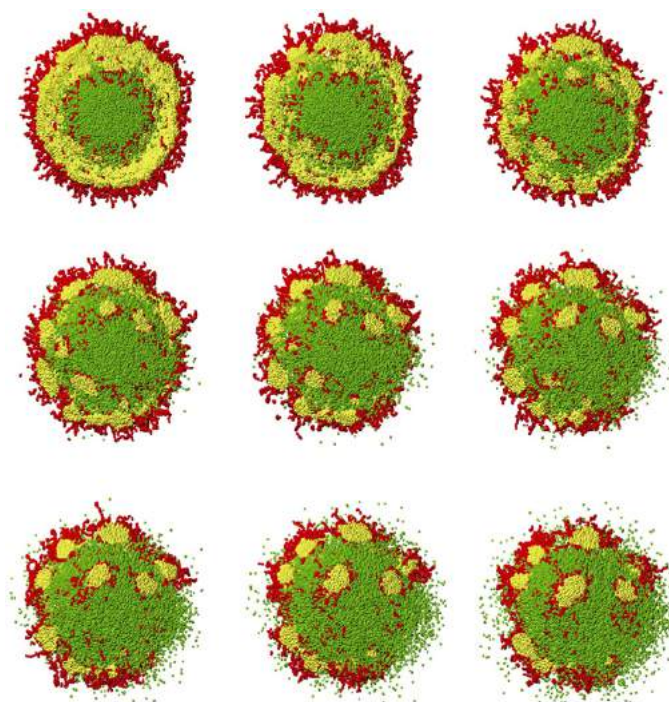
Figure 3. Sequence of snapshots of an explicit-solvent DPD simulation of a 28 nm diameter polymersome rupturing after being inflated with excess internal solvent. Note that solvent particles initially outside the polymersome are invisible for clarity while those inside are coloured green. The architecture of the polymers maps onto a PEO40–PEE37 diblock copolymer. Atomistic MD simulations were used to determine the equilibrium diblock bond lengths and angles, and these data were subsequently used to parametrize the DPD simulation. The vesicle contains 1569 diblock copolymers with an area per molecule approximately three times the relaxed value. The excess pressure drives the internal solvent into the inner leaflet, which then micellizes and subsequently weakens the outer leaflet. Multiple pores then appear, through which the solvent escapes into the external space. This vesicle is at the lower end of the physical size range for polymersomes, and the curvature stress in the membrane may be influencing the rupture pathway. (Figure reproduced from Ortiz *et al* (2005) with permission.)

1569 diblock copolymers ruptures after being inflated with excess internal solvent. The first step in the rupture pathway appears to be micellization of the inner leaflet, which subsequently weakens the outer leaflet, allowing the solvent to escape to the external volume via multiple pores.

This section shows that it is not always straightforward to apply the DPD technique to new systems. The coarse-graining procedure outlined in this sub-section, and the use of experimental data and results from atomistic MD simulations, provide a systematic and extensible method to calibrate the parameters required for a typical DPD simulation.

3.2. Tension-induced vesicle fusion

The key steps leading to membrane fusion are close proximity of the two membranes; initial contact and inter-penetration of the outer leaflets; opening of a pore connecting both membranes; and release of the vesicle contents. The fusion of two planar membranes appears to provide the simplest geometry for simulating membrane fusion, but has an implicit problem. The periodic boundary conditions that are commonly used result in the volume of solvent

between the two fusing membranes being constant until the fusion pore opens to allow the solvent to flow into the spaces behind the fusing membranes. This constant-volume constraint may influence the dynamics of the process, not least in requiring that the two membranes be initially so close together that they are effectively dehydrated along their whole surface. Placing a vesicle near a planar membrane avoids this difficulty as the solvent can flow around the vesicle in response to any local fluctuations of its shape. Fusion of a vesicle to a planar membrane also provides a better model for synaptic vesicle fusion in which a small, 40 nm diameter vesicle fuses to the much larger pre-synaptic membrane of the nerve cell.

The simplest driving force for membrane fusion is tension. Increasing the tension in a membrane results eventually in its rupture. If an alternative pathway is possible, such as merging with a closely apposed, less tense membrane, the rupture end-point can be avoided. We have recently studied this case in detail using DPD simulations (Shillcock and Lipowsky 2005) and summarize our results here. We note that the membranes used here are significantly more stretchable than typical lipid membranes, and are more similar in this respect to those formed of diblock copolymers. However, the model system captures the features that we believe are important for understanding the molecular rearrangements that occur during the fusion of tense membranes.

In this fusion protocol, a tense, 28 nm diameter vesicle is placed close to a tense 50×50 nm^2 planar membrane in a solvent-filled box. A small, solvent-filled gap of 1–2 nm separates them. When the vesicle is relaxed it contains approximately 6500 amphiphiles, and the relaxed planar membrane contains around 8200 amphiphiles. Such system sizes are an order of magnitude larger than any published atomistic, or coarse-grained, molecular dynamics fusion study. The global tensions in the vesicle and planar membrane are used as control parameters to explore the most probable evolutionary pathways for the system. These tensions are created by appropriately choosing the number of molecules in each membrane. The intact vesicle has a constant volume, as very few solvent molecules emerge on the timescale of the simulations compared to the approximately 50 000 initially inside it (see figures 1, 4 and 7). Repeating the protocol for each tension pair, using thermodynamically equivalent, but molecularly distinct, initial states, allows the probability of the various outcomes to be obtained. A typical fusion event is presented as a series of snapshots in figure 4. It can be seen that after the initial contact there is a rapid transfer of molecules from the vesicle to the *cis* leaflet of the (more tense) planar membrane, which destabilizes the merged contact zone, and leads to the fusion pore. Once the pore has been created, it grows rapidly due to the large tension present in the planar membrane.

The morphology diagram shown in figure 5 summarizes the outcomes of 93 independent fusion attempts. The areas per molecule for the planar membrane and vesicle are plotted along the X and Y axes respectively, and these quantities are monotonically related to the tensions. Several outcomes are shown in this diagram ranging from adhesion of the vesicle to the planar membrane at zero or low tension (shown as green dots); through a hemifused state in which the *cis* leaflets of the two membranes merge but their *trans* leaflets remain distinct until flip-flop of amphiphiles from one leaflet to the other causes them to merge (yellow dots); premature rupture of one or both membranes prior to fusion (red dots); and, finally, successful fusion (blue dots.) Further discussion of this diagram is given in our previous work (Shillcock and Lipowsky 2005) and its accompanying online supplementary information.

The first observation about fusion in this model is that it only occurs for membrane tensions not far removed from the membranes' stability limits. This reflects the presence of alternative pathways that compete with the fusion process to relax the initial tensions. These pathways are the rupture of one or both membranes, and their hemifusion.

Second, the 42 successful fusion events out of 93 attempts all occurred between 150 and 350 ns after initial contact of the two membranes even though the simulations were run out
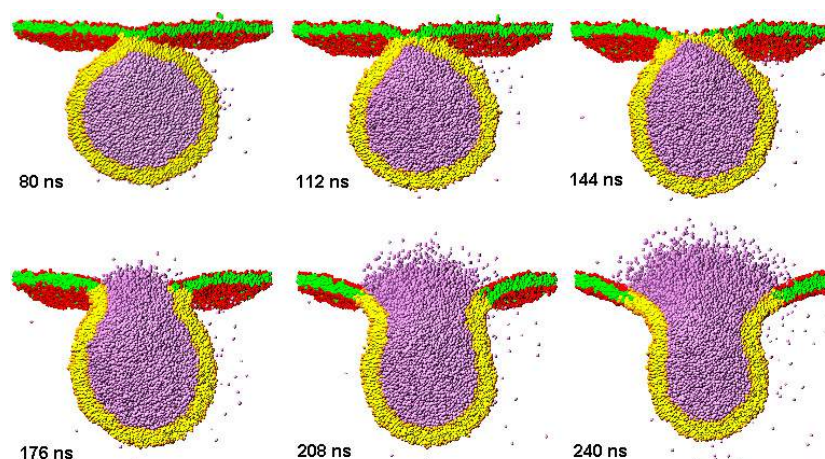
Figure 4. Time sequence of six snapshots for a typical fusion event of a tense 28 nm diameter vesicle and a tense square membrane patch, of linear extent 50 nm, containing 5684 and 5455 lipids respectively driven by the uniform initial tensions in the vesicle/planar membrane. The corresponding areas per lipid are $A/Na_0^2 = 1.9$ and 1.45 for the planar membrane and vesicle, respectively (upper right corner in figure 5). Particles representing groups of water molecules initially outside the vesicle are invisible for clarity, while those initially inside the vesicle are shown. Cross-sectional images through the simulation box are shown at 32 ns intervals, with the first image generated 80 ns after the start of the simulation. The initial contact of the vesicle to the planar membrane is via its shape fluctuations, and a few vesicle lipids are drawn across the solvent-filled gap of 1.2 nm into the planar membrane by its tension. The rare occurrence of a lipid spontaneously leaving the planar membrane and re-entering it is visible in the first two snapshots. The slow emergence of water particles from the vesicle interior is also visible prior to fusion, although the number that leave on the fusion timescale ($\sim$20) is again negligible compared to the number initially inside the vesicle ($\sim$50 000). (Figure reproduced from Shillcock and Lipowsky (2005).)

to 2 μm. The fusion time is defined here as the simulation time between the first contact of the two membranes and the time when the pore has expanded approximately to the diameter of the vesicle. Additionally, when the fusion times are binned according to the tension in the vesicle, the distributions all overlap considerably. The upper cut-off of the fusion time distribution arises from the stabilization of the hemifused state in the membrane geometry used here. Because the hemifused state is metastable for relatively large initial tensions, fusion can occur only at even higher tensions for which the fusion pathway exhibits no activation barrier. The stabilization of the hemifused state depends on the membrane areas that are initially stretched: if the vesicle and planar membrane areas are comparable, the planar membrane can relax its (higher) tension by incorporating vesicle amphiphiles before a fusion pore can appear. If the planar membrane area is much larger than the vesicle area, the hemifused states are only stabilized for smaller initial tensions, and the region of successful fusion is shifted towards smaller tensions.

We have verified this prediction for our vesicle–planar membrane geometry by performing ten additional simulations of the fusion of a small vesicle of diameter 14 nm to the same 50×50 nm² planar membrane. We choose a point in the lower right of the morphology diagram for which the initial areas per molecule are $A/Na_0^2 = 1.9$ and 1.3 for the planar membrane and vesicle respectively. Whereas the original ten independent simulations at this point result in the hemifused state, the smaller vesicle successfully fuses to the planar membrane in all ten new attempts. The mean fusion time of the ten new runs is 176 ns, which is within the range
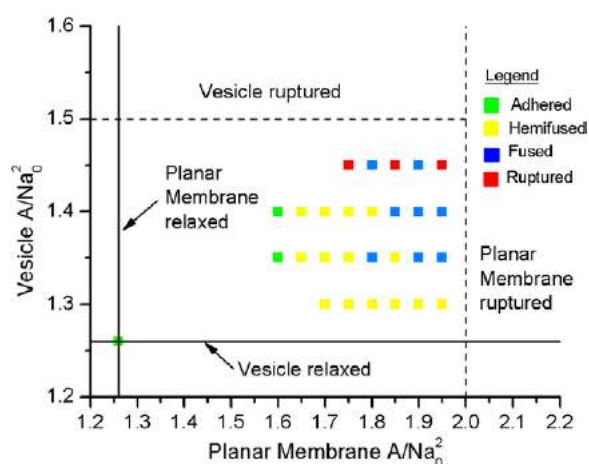
Figure 5. Morphology diagram for a vesicle in close proximity to a planar membrane as a function of the initial areas per lipid, A/Na_0^2, for the planar membrane and vesicle. The tensionless states are indicated by solid lines at the lower left of the diagram, and the area per lipid, at which rupture occurs almost immediately, by dashed lines at the upper right. Because rupture is a dynamic process, occurring more slowly as the tension is reduced, the rupture boundaries represent the area per lipid at which the vesicle or planar membrane were always observed to rupture within 2 μm. Points in the diagram are coloured according to the outcome that occurred in an absolute majority of the attempts: successful fusion is indicated by blue squares; rupture of the vesicle or planar membrane is indicated by red squares; hemifusion is indicated by yellow squares; and adhesion of the vesicle to the planar membrane, but without merging of their proximal monolayers, is indicated by green squares. Fusion of the vesicle to the planar membrane only occurs for initial areas per lipid within ~15% of the rupture boundaries, and even then is successful in at most ~50% of the attempts. Note that most squares represent the majority outcome of at least four independent simulations. Borderline cases were more intensively examined, e.g., ten runs of 1.6 μs each were performed for the point with the vesicle $A/Na_0^2 = 1.3$ and planar membrane $A/Na_0^2 = 1.9$, and seven runs of 640 ns for the point the with vesicle $A/Na_0^2 = 1.45$ and planar membrane $A/Na_0^2 = 1.75$. A total of 93 independent runs was performed to generate the data represented in this diagram. (Figure reproduced from Shillcock and Lipowsky (2005).)

found for the larger vesicle at the same tension (see figure 4 of Shillcock and Lipowsky 2005), indicating that the fusion time does not depend strongly on vesicle size.

These results show that modulating the global tensions in a vesicle–planar membrane system is an unreliable means of inducing their fusion because the required tensions, which need to be large so as to raise the probability of fusion, also allow the system to explore alternative mechanisms for releasing this tension, such as premature rupture of the vesicle or planar membrane. A more realistic fusion protocol is to embed model proteins in initially tensionless membranes, and to explore their possible actions in driving the membranes to fuse. Can protein-generated forces localized in space and time drive closely apposed, initially tensionless membranes to fuse? We address this question in the next section.

3.3. Vesicle fusion induced by model transmembrane proteins

Synaptic vesicle fusion *in vivo* is regulated and controlled by proteins (Mayer 2002, Jahn *et al* 2003, Ungermann and Langosch 2005). First, proteins transport the vesicles to their destination (Pfeffer 1999), where a different set of proteins, collectively called SNAREs (soluble N-ethylmaleimide-sensitive factor attachment protein receptor), both constrain the synaptic vesicles close to the pre-synaptic membrane of nerve cells and drive them to fuse (Carr

and Novick 2000). Although many SNARE proteins have been discovered, and some of their molecular structures are known (Ybe *et al* 2000), their mode of action is not yet understood (Weimer and Jorgensen 2003). In synaptic vesicle fusion, the membrane itself may play a regulatory role (Kweon *et al* 2003). There is still some controversy over whether the fusion pore in exocytosis is primarily lipidic, partially or completely lined by proteins (Lindau and Almers 1995, Han *et al* 2004), or if it transforms from one type to the other as it enlarges (Szule 2004, Han and Jackson 2004). There are several sub-stages even within the final fusion event (Jahn *et al* 2003). First, SNAREs on apposed membranes bind to each other. This stage provides the specificity that regulates fusion events, and directs vesicles to fuse only with the appropriate target membrane. Next, on receipt of a calcium signal, the extra-cellular segments of the SNAREs form a long coiled coil that 'zips' up starting at its distal end. This draws the two membranes together. Finally, a perturbation is effected in the tightly apposed membranes that creates the fusion pore and causes it to expand. It is on this final stage that mesoscopic simulations may shed some light.

Here, we ask the question of what perturbation the transmembrane anchors of the SNARE proteins could create that promotes formation and expansion of the fusion pore. This question is also relevant to viral fusion, in which a virus connects via a hydrophobic piece of a viral envelope protein with its target membrane (Jahn *et al* 2003, Pascual *et al* 2005). Our fusion mechanism is simple, involving only a number of rigid, membrane-spanning inclusions, or *barrels*, to which external forces can be applied, and which transduce these forces into the surrounding membrane.

Experiments on *in vitro* assays of SNARE-mediated fusion have shown that passively holding a vesicle close to its target membrane is not sufficient for fusion to occur: the proteins appear to exert forces via their transmembrane anchors (McNew *et al* 2000). SNARE proteins have a transmembrane segment to which is attached the extracellular strand that forms a coiled coil when joined by its cognate SNAREs. If the transmembrane segment is replaced by a simple lipid anchor, the mutant SNARE is unable to effect fusion. However, if the tail length of the lipid anchor is increased to equal the width of the membrane, fusion activity is restored (McNew *et al* 2000). This suggests that the protein requires a minimum degree of anchoring strength for it to function. This conclusion is supported by recent atomistic molecular dynamics simulations (Knecht and Grubmüller 2003) of a piece of the transmembrane segment of the SNARE protein syntaxin 1A. These simulations show that it can transduce a significant force between its component parts. If this force were to stretch the surrounding membrane it could help to create a fusion pore. Yersin *et al* (2003) have used atomic force microscopy to measure the maximum force sustainable by a reconstituted SNARE complex. They found that forces up to two hundred piconewtons can be sustained by the complex without it disintegrating. A theoretical model based on these results predicts that a minimum of four complexes is needed to hold a vesicle close to its target membrane.

We use these results to hypothesize that a number of SNARE proteins, whose transmembrane segments are arranged in a circle, act co-operatively to transduce forces to the membrane in which they are anchored, resulting in a local bending and stretching of the merged lipid bilayers. As the SNARE complexes form, they bend the two membranes together until their outer leaflets mingle, and then raise the tension within the merged zone until a fusion pore develops. We use DPD simulations to explore the application of external forces to 12 transmembrane barrels (six in each membrane), each with a diameter of about 2 nm, arranged in a circle whose radius is varied around 6 nm, and to measure the work required to stretch the enclosed region of membrane until a pore appears. Note that the length scale in these simulations is obtained by equating the area per molecule in a tensionless membrane to that of a typical phospholipid (0.6 nm^2) as in our previous work. This yields the equivalence that
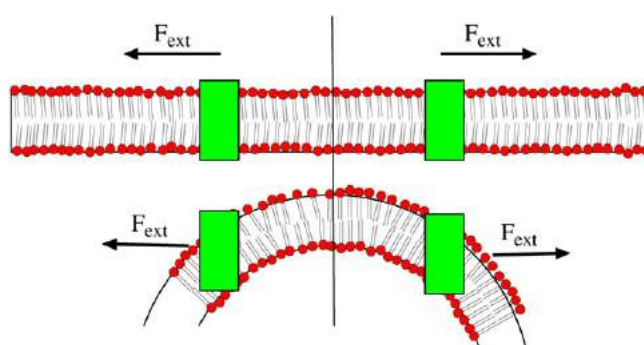
Figure 6. Cartoon showing how the transmembrane 'barrels', which represent the transmembrane portions of SNARE proteins, are constructed by polymerizing a cylinder of amphiphiles in a membrane. The cylinders typically have a radius of $1.5a_0$, and are positioned in an annulus of radius $8a_0$, where a_0 is the DPD bead diameter. Their length is fixed as the distance between the amphiphile headgroups in opposite monolayers of the membrane. Six barrels are created in each membrane. Because of the vesicle's curvature the amphiphiles forming the barrels in the vesicle membrane are not completely polymerized, but we do not expect this significantly to modify the results. Each barrel contains on average 80–90 beads. Once the barrels have been defined, external forces are applied to (the beads defined within) them, causing them to move in the membrane plane and drag a small patch of surrounding amphiphiles with them. The forces are directed radially outwards, thereby raising the tension in the circular membrane patch enclosed by the barrels. This tension increases the probability of a pore being formed in this patch.

one bead diameter $a_0 = 0.7$ nm. The timescale is obtained by comparing the lipid in-plane diffusion coefficient in the membrane to a typical experimental value ($5 \ \mu\text{m}^2 \ \text{s}^{-1}$), also as used before. This results in 1000 time-steps being equivalent to 16 ns. We measure the work done as a function of the magnitude of the applied force, and explore its dependence on the diameter and location of the barrels. The motivation for the number of barrels is that six SNARE complexes is at the mid-range of the number predicted in the model of Yersin *et al* (2003), and a protein/lipid ratio of 1:100 is used in a recent *in vitro* fusion assay on 30 nm diameter vesicles (Schuette *et al* 2004). The vesicle in our simulations has a diameter of 28 nm and contains 5887 lipids. It would contain on average 60 SNARE complexes distributed uniformly over its surface in the assay of Schuette *et al* (2004), and would have a mean area per complex of 42 nm², or a mean separation of 6.5 nm. Creating these transmembrane barrels is straightforward in particle-based simulations, and we describe our method next.

Several recent papers have reported simulations of inclusions in membranes as computational models of experimental systems. Such models range from atomistic MD simulations of a bundle of alpha-helices that form part of an ion channel (Appelt *et al* 2005, Saiz and Klein 2005), to coarse-grained MD simulations of transmembrane hydraphiles (Srinivas *et al* 2004b), and DPD simulations quantifying the effects of the hydrophobic mismatch of a barrel-shaped protein inserted in a fluid membrane (Venturoli *et al* 2005). We create a rigid, barrel-shaped, transmembrane protein whose size is matched to the surrounding membrane by selecting the amphiphiles in a cylindrical region of the membrane and tying their beads together using stiff Hookean springs as illustrated in figure 6. The radius of the cylinder is variable but its length is chosen to equal the membrane width. The bead–bead interactions of the barrel are therefore matched with those of the surrounding amphiphiles and solvent by construction. Any number of transmembrane barrels may be created, as long as no two overlap. External forces may be applied to the barrels by adding a term to the equations of motion for those beads that comprise the barrels. Energy is not conserved in DPD due to the thermostat provided by the
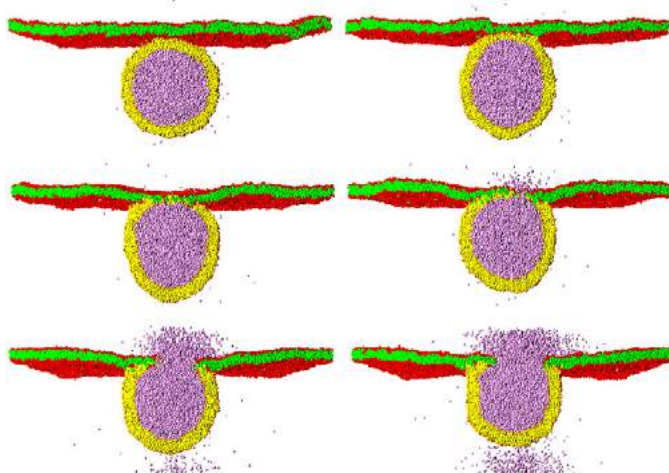
Figure 7. Sequence of snapshots of a 28 nm diameter vesicle fusing with a 100×100 nm^2 planar membrane patch. Both membranes are tensionless. Six membrane-spanning barrel 'proteins' are positioned in an hexagonal arrangement in each. The proteins are constructed by 'polymerizing' a cylinder of amphiphiles using stiff Hookean springs. The resulting rigid inclusions have bead–bead interactions matching their surrounding membrane environment. A specific force protocol is applied to these barrels in order to drive the membranes to fuse. After the membranes have equilibrated, oppositely oriented bending moments are created in each membrane for 80 ns to bend them towards each other. Once the membrane proximal leaflets have touched, the bending moments are removed and the system allowed to evolve 32 ns in order for the two proximal leaflets to merge somewhat. An external force is then applied to the barrels in both membranes so as to raise the tension in the encircled contact zone. The force has magnitude $F_{\text{ext}} = 0.4k_{\text{B}}T/a_0$ and is directed radially outward. It is applied in this instance for 64 ns. Once the pore has appeared it expands under the pressure of the inner solvent flowing outwards, but as the membranes relax back to their tensionless states the pore shrinks.

random and dissipative forces. Providing the external force is not so large as to interfere with the temperature regulation of the thermostat, it acts simply to increase locally the momentum of a set of particles.

Two effects limit the magnitude of the force that may be applied to the barrels. Because the membrane is in a fluid state, if the external force is decreased to the point at which its effects are comparable to the thermal motion of the amphiphiles, it can do no useful work on the membrane. Forces only somewhat larger than the thermal force, for which the barrel protein displacement increases slowly, allow the lipids to rearrange around the barrel as it moves, and the perturbation is limited to those amphiphiles immediately adjacent to the barrel. At the opposite extreme, if the applied force is large, the membrane cannot rearrange quickly enough to follow the barrel's motion, and the barrel is likely to be pulled out of the membrane. There is therefore a regime, which is bounded above and below, in which the force creates a perturbation in the membrane for some distance around the barrel that persists as long as the force is applied.

The first step in this fusion protocol is to bring the two membranes into contact. We use an *ad hoc* mechanism to bend the membranes towards each other. A bending moment is created in each membrane by modulating the bead–bead interactions of the lipid headgroups in apposed annuli in the two leaflets of the membrane. Creating two such moments of opposite sign in adjacent membranes causes the circular regions of membrane bounded by the annuli to move towards each other (see snapshot 2 of figure 7.) Once they touch, amphiphiles can start to cross over to the adjacent membrane. When the membranes are in contact, the modified bead–bead

interactions are restored to their original values, and the bending moment disappears. Because we make this change in an annulus some distance away from the centre of the contact zone, 5.6–11.2 nm, and the modified beads are restored to their original state before the stretching force is applied, we believe that the only effect of this step on the fusion process is transiently to bend the membranes towards each other until their *cis* leaflets touch.

In the next step, the *cis* leaflets of the membranes are allowed to merge for a set period of time, and then an external force is applied to the 12 barrels (six in each membrane) that form a ring around the contact zone. The magnitude and duration of the force, as well as the size and location of the barrel proteins in the membranes, are parameters of the protocol. The stretching force is directed radially outwards in the plane of the membranes. After the specified duration, the external force is removed and the simulation allowed to evolve freely for the remainder of the run. A minimum delay before turning on the stretching force is found to be crucial to forming a membrane-spanning pore. If the bending and stretching forces are too closely spaced in time, so that the *cis* leaflets have not had time to merge, the effect of the latter is simply to return the two membranes to their original, flat, non-contacting states. The time required to create the fusion pore is measured from the first contact of the membranes to the time when the pore, if one appears, has grown to approximately the diameter of the vesicle.

We quantify the effects of the external force by calculating its path integral as it displaces each barrel protein. The vector displacement of each bead during each time step for which the force is non-zero is multiplied by the vector force and the resulting $F \cdot dx$ terms summed over all beads in all 12 barrels to give the total work done. The total vector displacement of each barrel is also measured. This allows the work transduced by each barrel into the membrane to be calculated. We mention here again that the membranes used in these *in silico* fusion experiments are more stretchable than actual lipid bilayers, and that this will influence the magnitude of the work required to open a pore. The fusion of membranes whose elastic properties are closer to those of lipid vesicles are currently under investigation, but we believe that the observed dependence of the work done on the magnitude and duration of the applied force, and the size and location of the transmembrane barrels, is relevant for all protein-induced membrane fusion models.

Forces of magnitude $F = 0.3$–$0.5k_B T/a_0$ (equivalent to 160 pN per barrel, given that each one contains approximately 80 beads) are found to reproducibly open a pore in the membranes, whereas smaller forces frequently fail. There is a systematic decrease in the work required to open a pore as the force decreases. The minimum value we have so far observed is $90k_B T$ per barrel protein, or the equivalent of hydrolysing four to five ATP molecules. The distance moved by each barrel is approximately 8 nm (equivalent to four times the barrel diameter). In a typical fusion event, the bending force is exerted for 80 ns, followed by a 32 ns lag period to allow the *cis* leaflets to partially merge. Then the pulling force is applied for approximately 64 ns and the pore requires a further 80 ns to expand. This gives a fusion pore time of around 250 ns.

This fusion protocol can clearly be further optimized. If more barrels are used to transduce the external force into the membrane, the work done by each will be reduced. We have started to explore the effects of changing the barrel size and location. As the diameter of the barrels decreases, the reliability of fusion pore formation decreases. For barrels of diameter 2.1 nm arranged in annuli of radius 4.2–5.6 nm a fusion pore always forms after application of the force, whereas for barrels of diameter 1.7 nm the fusion pore forms in less than one-half of the attempts. Increasing the radial separation of the barrels to 7 nm also reduces the work done. However, beyond this distance, the fusion pore frequently fails to form. Successful fusion therefore requires a minimum barrel size, presumably to ensure that the perturbation is applied to a sufficiently large segment of the membrane; and the barrels must be arranged in a circle whose radius is also constrained to lie within limits. A further reduction in the work done

can be obtained by reducing the duration of the applied force. The decreasing work expended in pulling the barrels through the membrane with decreasing force is easily explained as less energy is dissipated into the surrounding fluid membrane.

4. Discussion and outlook

The goal of mesoscale modelling is to capture just those interactions of a system that are necessary and sufficient to allow the prediction of the properties of interest at a lesser cost in time and resources than the equivalent experiments or atomistically detailed MD simulations. Such predictions can then be used to direct attention, and costly computational resources, towards the regions of a model's parameter space that provide the best hope of yielding insight into experimental processes. As industrial demand grows for the ability to design smart biomaterials possessing increasingly finely tuned properties, coarse-grained computer simulations provide one of the clearest roads to satisfy this need. The design of biomimetic membranes that modify their properties in response to external signals, and can be used to construct artificial cells, is now feasible.

The use of mesoscale simulations to understand biological membranes is an ongoing process that may be divided into three stages: assembly–response–control. Early applications followed the self-assembly of amphiphilic molecules in aqueous solvent into aggregates such as micelles, planar bilayers and vesicles. Several groups are now systematically exploring how these aggregates, especially vesicles and bilayers, respond to changes in the interaction parameters between the molecular species. The aggregates' responses are typically characterized using equilibrium properties, such as the area per molecule, bilayer thickness, membrane area stretch modulus and bending stiffness, and in-plane diffusion coefficients. The response of membranes to the presence of mimics of alpha-helical peptides and other membrane-penetrating molecules has been studied using a molecular-level mean field theory (Zemel *et al* 2004), coarse-grained MD (Srinivas *et al* 2004a, 2004b) and DPD (Venturoli *et al* 2005), and even atomistic MD (Appelt *et al* 2005, Saiz and Klein 2005). These embedded molecules can act as centres for the application of external forces, or their presence alone can induce perturbations, that drive the membrane along pathways mimicking active processes in biological membranes. The modelling of active processes in membranes is crucial, as biophysical processes in cells are typically maintained far from equilibrium. Transitions between states are frequently activated processes that depend sensitively on some parameter, as the appearance of a pore in a tense membrane depends exponentially on the pore's line tension. Combining methods that increase the sampling of rare transition events (Bolhuis *et al* 2002, Allen *et al* 2006) with a coarse-grained model of the membrane allows such rare transition events to be more efficiently sampled than performing unbiased simulations alone. As simulations of membrane–protein interactions are developed further, they will reveal the molecular rearrangements occurring during even less-understood fusion processes such as *in vitro* (Hu *et al* 2003) and *in vivo* (Chen and Olson 2005) cell–cell fusion. Recent experiments exploring the effects of fusion peptides on membrane structure and stability (Haque *et al* 2005), and the opportunity to simulate such systems at comparable length- and timescales, will undoubtedly lead to new insights.

Clinical applications of particle-based membrane simulations include designing better drug delivery systems (Chang 2005). Polymersomes or lipid vesicles containing active ingredients can be simulated as they expel their contents into the surrounding solvent. The influence of molecular changes in membrane constituents can be explored systematically, and desirable properties enhanced. Such simulations must be able to capture behaviour on length-scales of hundreds of nanometres, which makes coarse-grained techniques, such as DPD, important tools

in this area. We have summarized recent simulation results (Ortiz *et al* 2005) that show that the usual DPD mapping from atomistic particles to coarse-grained beads must be modified if the polymersome's physical properties are to be correctly reproduced in the DPD simulation. The DPD technique itself is still evolving, and new thermostats have recently been proposed (Stoyanov and Groot 2005) to improve the temperature control and to allow a wider variation in fluid properties such as viscosity. This suggests that there is still work to be done in applying DPD to novel systems.

In a biological context, mesoscale simulations of membranes, protein–membrane interactions, and active processes such as force transduction may lead to new insights into processes such as viral penetration of cells, the interactions of multiple molecular species in the confined, membrane-bounded environments of the cell, and the control or remodelling of membranes by active processes occurring in or near the membrane. We have used DPD simulations to study the fusion of a vesicle to a planar membrane driven by forces that are localized in space and time. The process is found to consume about $100k_BT$ per barrel protein. The time required for the fusion pore to be created and grow to the vesicle diameter is of the order of 300 ns, which is not dissimilar to the values of 200–300 ns found in our previous work (Shillcock and Lipowsky 2005) in which a global tension is used to create the fusion pore. This is several orders of magnitude smaller than the 25 ms duration observed in *in vitro* assays of SNARE-driven fusion of a vesicle with a planar lipid bilayer (Liu *et al* 2005). This timescale is clearly related to the membrane's viscoelastic properties. We note that the sharp boundary between the fused vesicle and planar membrane indicates that the amphiphiles have not had time to diffuse far from the pore edge while the pore is forming. This can be seen in figures 1 and 7, where the boundary between amphiphiles originating in the two membranes is still sharper than a few bead diameters. A typical phospholipid lateral diffusion coefficient is $5 \ \mu m^2 \ s^{-1}$, indicating that a lipid requires approximately 100 ns to diffuse its own diameter. This yields an estimate of several hundred nanoseconds for the lipids to diffuse a few diameters, which supports the short pore lifetimes we observe.

Exploring the origin of this disparity in fusion times using a variety of mesoscopic models (DPD, coarse-grained MD, etc) will yield insight into possible active mechanisms of SNARE proteins. We are currently exploring the fusion of membranes in DPD simulations whose elastic properties more closely reflect those of lipid bilayers, and find that the typical time to form a fusion pore is an order of magnitude larger for membranes that can only support 20% area stretch before rupturing (unpublished data). However, part of the large gap between experimental fusion times and those predicted from simulations may be due to the complexity of experimental fusion protocols. These measure not just the time required for fusion pore formation, but also a signalling time (often a calcium signal) that initiates the fusion process, the time required for the protein conformational changes that perturb the membranes, and the fusion pore growth time until a signal can be measured. It is the sum of all these times that makes up the *in vitro* 25 ms fusion time. Mesoscopic simulations allow one to focus on distinct stages in the fusion process, and observe molecular-scale processes that cannot be seen in experiments. Tuning the model parameters using experimental results is a key part of the process of suitably applying such models to complex biophysical processes.

In order to realize the full promise of mesoscale models, we suggest some key further developments that are required. The system sizes and times currently reachable using coarse-grained models are perhaps a few hundred nanometres for a few microseconds, as shown in this work, or tens of nanometres for hundreds of microseconds (Stevens *et al* 2003). Many biological processes require system sizes of at least several cubic microns to be simulated for times reaching up to milliseconds if not seconds. The development of parallel codes is essential to reach such scales, and a combination of simulation techniques is required. Multi-scale

modelling techniques (Fabritiis *et al* 2002) have recently attracted attention (Chang *et al* 2005, Izvekov and Voth 2005, Kremer 2005, Shi and Voth 2005). Models attempting to simulate the behaviour of a complete cell membrane, including its growth due to incorporating new material, are already being developed (Broderick *et al* 2004), and raise the tantalizing possibility of being able to simulate a whole bacterium with near-molecular resolution.

It seems likely that in the future several techniques will be combined into a 'multi-scale self-parametrizing model' in which key parameters for the larger length- and timescales are continuously determined from data generated at smaller scales. Coarse-grained simulation techniques are not destined to replace atomistic MD, but their combination within a single simulation code will usher in an era in which atomistically detailed MD simulations of small amounts of matter will feed larger computational models in a tool that is able to parametrize itself, and allow the study of systems in which interactions propagate continuously across many length and time scales. This tool will be of immense benefit in visualizing and rationally designing the smart biomaterials of tomorrow.

References

Allen R J, Frenkel D and ten Wolde P R 2006 *J. Chem. Phys.* **124** 024102
Antonietti M and Förster S 2003 *Adv. Mater.* **15** 1323
Appelt C, Eisenmenger F, Kühne R, Schmieder P and Söderhäll J A 2005 *Biophys. J.* **89** 2296
Besold G, Vattulainen I, Karttunen M and Polson J M 2000 *Phys. Rev.* E **62** 7611
Bolhuis P G, Chandler D, Dellago C and Geissler P L 2002 *Annu. Rev. Phys. Chem.* **53** 291
Bonnafous P and Stegmann T 2000 *J. Biol. Chem.* **275** 6160
Broderick G, Ru'aini M, Chan E and Ellison M J 2004 *In Silico Biol.* **5** 0016
Burke M G, Woscholski R and Yaliraki S N 2003 *Proc. Natl Acad. Sci.* **100** 13928
Canham P B 1970 *J. Theor. Biol.* **26** 61
Carr C M and Novick P J 2000 *Nature* **404** 347
Chang R, Ayton G S and Voth G A 2005 *J. Chem. Phys.* **122** 244716
Chang T M S 2005 *Nat. Rev. Drug Discovery* **4** 221
Chanturiya A, Scaria P, Kuksenok O and Woodle M C 2002 *Biophys. J.* **82** 3072
Chemical Industry Vision2020 Technology Partnership *Technology Roadmap for Materials* chapter 4 (http://www.chemicalvision2020.org)
Chen E H and Olson E N 2005 *Science* **308** 369
Chernomordik L V and Kozlov M L 2005 *Cell* **123** 375
Cooke I R, Kremer K and Deserno M 2005 *Phys. Rev.* E **72** 011506
Den Otter W K and Clarke J H R 2001 *Europhys. Lett.* **53** 426
De Vries A H, Mark A E and Marrink S-J 2004 *J. Am. Chem. Soc.* **126** 4488
Discher B M, Won Y Y, Ege D S, Lee J C M, Bates F S, Discher D E and Hammer D A 1999 *Science* **285** 1143
Discher D E and Eisenberg A 2002 *Science* **297** 967
Espagnol P and Warren P 1995 *Europhys. Lett.* **30** 191
Evans E A 1974 *Biophys. J.* **14** 923
Fabritiis G de, Coveney P V and Flekkoy E G 2002 *Phil. Trans. R. Soc.* A **360** 317
Falck E, Patra M, Karttunen M, Hyvönen M T and Vattulainen I 2004 *Biophys. J.* **87** 1076
Farago O 2003 *J. Chem. Phys.* **119** 596
Farago O 2005 *J. Chem. Phys.* **122** 044901
Fix M, Melia T J, Jaiswal J K, Rappoport J Z, You D, Söllner T H, Rothman J E and Simon S M 2005 *Proc. Natl Acad. Sci. USA* **101** 7311
Flekkoy E G and Coveney P V 1999 *Phys. Rev. Lett.* **83** 1775
Fournier L and Joos B 2003 *Phys. Rev.* E **67** 051908
Frolov V A, Dunina-Barkovskaya A Y, Samsonov A V and Zimmerberg J 2003 *Biophys. J.* **85** 1725
Gingell D and Ginsberg I 1978 *Membrane Fusion* ed G Poste and G L Nicolson (New York: Elsevier)
Goetz R and Lipowsky R 1998 *J. Chem. Phys.* **108** 7397
Goetz R, Gompper G and Lipowsky R 1999 *Phys. Rev. Lett.* **82** 221
Gompper G and Kroll D M 1997 *J. Phys.: Condens. Matter* **9** 8795
Groot R D 2000 *Langmuir* **16** 7493

Groot R D 2003 *J. Chem. Phys.* **118** 11265

Groot R D and Madden T J 1998 *J. Chem. Phys.* **20** 8713

Groot R D and Rabone K L 2001 *Biophys. J.* **81** 725

Groot R D and Warren P B 1997 *J. Chem. Phys.* **107** 4423

Haluska C K, Riske K A, Marchi-Artzner V, Lehn J-M, Lipowsky R and Dimova R 2006 *Proc. Natl Acad. Sci. USA* submitted

Han X and Jackson M B 2004a *Science* **306** 813c

Han X, Wang C-T, Bai J, Chapman E R and Jackson M B 2004b *Science* **304** 289

Haque M E, Koppaka V, Axelsen P H and Lentz B R 2005 *Biophys. J.* **89** 3183

Helfrich W 1973 *Z. Naturf.* c **28** 693

Hofsäss C, Lindahl E and Edholm O 2003 *Biophys. J.* **84** 2192

Holopainen J M, Lehtonen J Y A and Kinnunen P K J 1999 *Biophys. J.* **76** 2111

Hoogerbrugge P J and Koelman J M V A 1992 *Europhys. Lett.* **19** 155

Hui S E, Stewart T P, Boni L T and Yeagle P L 1981 *Science* **212** 921

Hu C, Ahmed M, Melia T J, Süllner T H, Mayer T and Rothman J E 2003 *Science* **300** 1745

Hyvönen M T and Kovanen P T 2003 *J. Phys. Chem.* B **107** 9102

Illya G, Lipowsky R and Shillcock J C 2005 *J. Chem. Phys.* **122** 244901

Irfachsyad D, Tildesley D and Malfreyt P 2002 *Phys. Chem. Chem. Phys.* **4** 3008

Izvekov S and Voth G A 2005 *J. Phys. Chem.* B **109** 2469

Jahn R and Grubmüller 2002 *Curr. Opin. Cell Biol.* **14** 488

Jahn R, Lang T and Südhof T 2003 *Cell* **112** 519

Jakobsen A F 2005 *J. Chem. Phys.* **122** 124901

Jakobsen A F, Mouritsen O G and Besold G 2005 *J. Chem. Phys.* **122** 204901

Jones J L, Lal M, Ruddock J N and Spenley N A 1999 *Faraday Discuss.* **112** 129

Katsov K, Müller M and Schick M 2005 *Biophys. J.* **87** 3277

Kiessling V 2005 *Biophys. J.* **89** 2185

Kinnunen P K J and Holopainen J M 2000 *Biosci. Rep.* **20** 465

Knecht V and Grubmüller H 2003 *Biophys. J.* **84** 1527

Kozlov M M and Markin V S 1983 *Biofizika* **28** 242

Kozlovsky Y and Kozlov M M 2002 *Biophys. J.* **82** 882

Kranenburg M, Venturoli M and Smit B 2003 *Phys. Rev.* E **67** 060901R

Kremer K 2005 *Handbook of Materials Modeling* ed S Yip (Berlin: Springer) p 2675

Kumar P B S, Gompper G and Lipowsky R 2001 *Phys. Rev. Lett.* **86** 3911

Kuzmin P E, Zimmerberg J, Chizmadzhev J A and Cohen F S 2001 *Proc. Natl Acad. Sci.* **98** 7235

Kweon D-H, Kim C S and Shin Y-K 2003 *Nat. Struct. Biol.* **10** 440

Lei G and MacDonald R C 2003 *Biophys. J.* **85** 1585

Lentz B R, Siegel D P and Malinin V 2002 *Biophys. J.* **82** 555

Lindau M and Almers W 1995 *Curr. Opin. Cell Biol.* **7** 509

Lindau M and de Toledo G A 2003 *Biochim. Biophys. Acta* **1641** 167

Lipowsky R 2004 *Nat. Mater.* **3** 589

Lipowsky R, Brinkmann M, Dimova R, Haluska C, Kierfeld J and Shillcock J C 2005 *J. Phys.: Condens. Matter* **17** S2885

Lipowsky R and Sackmann E (ed) 1995 Structure and dynamics of membranes-from cells to vesicles *Handbook of Biological Physics* vol 1A/1B (Amsterdam: Elsevier)

Lipowsky R and Zielinska B 1989 *Phys. Rev. Lett.* **62** 1572

Litster J 1975 *Phys. Lett.* A **53** 193

Liu T, Tucker W C, Bhalla A, Chapman E R and Weisshaar J C 2005 *Biophys. J.* **89** 2458

Lowe C P 1999 *Europhys. Lett.* **47** 145

Lu X, Zhang F, McNew J A and Shin Y-K 2005 *J. Biol. Chem.* **280** 30538

Markin V S and Albanesi J P 2002 *Biophys. J.* **82** 693

Markin V S, Kozlov M M and Borovjagin V L 1984 *Gen. Physiol. Biophys.* **3** 361

Marrink S-J, Lindahl E, Edholm O and Mark A E 2001 *J. Am. Chem. Soc.* **123** 8638

Marrink S-J and Mark A E 2003a *J. Am. Chem. Soc.* **125** 15233

Marrink S-J and Mark A E 2003b *J. Am. Chem. Soc.* **125** 11144

Marrink S-J and Tieleman D P 2002 *Biophys. J.* **83** 2386

Marrink S-J, Tieleman D P and Mark A E 2000 *J. Phys. Chem.* B **104** 12165

Mayer A 2001 *Trends Biochem. Sci.* **26** 717

Mayer A 2002 *Annu. Rev. Cell Dev. Biol* **18** 289

McNew J A, Weber T, Parlati F, Johnston R J, Melia T J, Sollner T H and Rothman J E 2000 *J. Cell Biol.* **150** 105

Melikyan G B, Barnard R J O, Abrahamyan L G, Mothes W and Young J A T 2005 *Proc. Natl Acad. Sci.* **102** 8728

Meng F, Engbers G H M and Feijen J 2005 *J. Control. Release* **101** 187

Müller M, Katsov K and Schick M 2003 *Biophys. J.* **85** 1611

Nikunen P, Karttunen M and Vattulainen I 2003 *Comput. Phys. Commun.* **153** 407

Noguchi H and Takasu M 2001a *Phys. Rev.* E **64** 041913

Noguchi H and Takasu M 2001b *J. Chem. Phys.* **115** 9547

Nomura F, Inaba T, Ishikawa S, Nagata M, Takahashi S, Hotani H and Takiguchi K 2004 *Proc. Natl Acad. Sci.* **101** 3420

Ohta-lino S, Pasenkiewicz-Gierula M, Takaoka Y, Miyagawa H, Kitamura K and Kusimi A 2001 *Biophys. J.* **81** 217

Ortiz V, Nielsen S O, Discher D E, Klein M L, Lipowsky R and Shillcock J C 2005 *J. Phys. Chem.* B **109** 17708

Palmer B J and Liu J 1996 *Langmuir* **12** 746

Pascual R, Moreno M R and Villalain J 2005 *J. Virol.* **79** 5142

Peters E A J F 2004 *Europhys. Lett.* **66** 311

Pfeffer S R 1999 *Nat. Cell Biol.* **1** E17

Prinsen P, Warren P B and Michels M A J 2003 *Phys. Rev. Lett.* **89** 148301

Rawicz W, Olbrich K C, McIntosh T, Needham D and Evans E 2000 *Biophys. J.* **79** 328

Rekvig L, Kranenburg M, Vreede J, Hafskjold B and Smit B 2003 *Langmuir* **19** 8195

Rosoff M (ed) 1996 *Vesicles* (*Surfactant Science Series* vol 62) (New York: Dekker) section II

Rozycki B, Lipowsky R and Weikl T 2006 *Phys. Rev. Lett.* **96** 048101

Saiz L and Klein M L 2005 *Biophys. J.* **88** 959

Schick M, Katsov K and Müller M 2005 *Mol. Phys.* **103** 3055

Schuette C G, Hatsuzawa K, Margittai M, Stein A, Riedel D, Küster P, König M, Seidel C and Jahn R 2004 *Proc. Natl Acad. Sci.* **101** 2858

Sens P and Safran S A 1998 *Europhys. Lett.* **43** 95

Sevink G J A and Zvelindovsky A V 2005 *Macromolecules* **38** 7502

Shangguan T, Alford D and Bentz J 1996 *Biochemistry* **35** 4956

Shelley J C and Shelley M Y 2000 *Curr. Opin. Colloid Interface Sci.* **5** 101

Shelley J C, Shelley M Y, Reeder R C, Bandyopadhyay S and Klein M L 2001 *J. Phys. Chem.* B **105** 4464

Shi Q and Voth G A 2005 *Biophys. J.* **89** 2385

Shillcock J C and Lipowsky R 2002 *J. Chem. Phys.* **117** 5048

Shillcock J C and Lipowsky R 2005 *Nat. Mater.* **5** 225

Shillcock J C and Seifert U 1998 *Biophys. J.* **74** 1754

Siegel D 1993 *Biophys. J.* **65** 2124

Siegel D 1999 *Biophys. J.* **76** 291

Singer S L and Nicholson G L 1972 *Science* **175** 720

Smit B, Hilbers P A J, Esselink K, Rupert L A M, van Os N M and Schlijper A G 1990 *Nature* **348** 624

Soddemann T, Dunweg B and Kremer K 2003 *Phys. Rev.* E **68** 046702

Srinivas G, Discher D E and Klein M L 2004a *Nat. Mater.* **3** 638

Srinivas G, Lopez C F and Klein M L 2004b *J. Phys. Chem.* **108** 4231

Stevens M J, Hoh J H and Woolf T B 2003 *Phys. Rev. Lett.* **91** 188102

Stoyanov S D and Groot R D 2005 *J. Chem. Phys.* **122** 114112

Symeonidis V, Karniadakis G E and Caswell B 2005 *Phys. Rev. Lett.* **95** 076001

Szule J A 2004 *Science* **306** 813b

Tamm L K, Crane J and Kiessling V 2003 *Curr. Opin. Struct. Biol.* **13** 453

Tieleman D P, Leontiadou H, Mark A E and Marrink S-J 2003 *J. Am. Chem. Soc.* **125** 6382

Tieleman D P, van der Spoel D and Berendsen H J C 2000 *J. Phys. Chem.* B **104** 6380

Tolpekina T V, den Otter W K and Briels W J 2004 *J. Chem. Phys.* **121** 8014

Torchilin V P 2005 *Nat. Rev. Drug Discovery* **4** 145

Ungermann C and Langosch D 2005 *J. Cell Sci.* **118** 3819

Venturoli M and Smit B 1999 *Phys. Chem. Commun.* **10** 1

Venturoli M, Smit B and Sperotto M M 2005 *Biophys. J.* **88** 1778

Vijayan K, Discher D E, Lal J, Janmey P and Goulian M 2005 *J. Phys. Chem.* B **109** 14356

Wang Z and Frenkel D 2005 *J. Chem. Phys.* **122** 234711

Warren P B 1998 *Curr. Opin Colloid Interface Sci.* **3** 620

Warren P B 2001 *Phys. Rev. Lett.* **87** 225702

Weimer R M and Jorgensen E M 2003 *J. Cell Sci.* **116** 3661

White J M and Castle J D 2005 *Nat. Struct. Mol. Biol.* **12** 382

Whittle M and Dickinson E 2001 *J. Colloid Interface Sci.* **242** 106

Xu Y, Zhang F, Su Z, McNew J A and Shin Y-K 2005 *Nat. Struct. Mol. Biol.* **12** 417

Yamamoto S and Hyodo S 2003 *J. Chem. Phys.* **118** 7937

Yamamoto S, Maruyama Y and Hyodo S 2002 *J. Chem. Phys.* **116** 5842

Ybe J A, Wakeham D E, Brodsky F M and Hwang P K 2000 *Traffic* **1** 474

Yersin A, Hirling H, Steiner P, Magnin S, Regazzi R, Huni B, Huguenot P, De Los Rios P, Dietler G, Catsicas S and Kasas S 2003 *Proc. Natl Acad. Sci.* **100** 8736

Zemel A, Ben-Shaul A and May S 2004 *Biophys. J.* **86** 3607

Zhou Y and Yan D 2005 *J. Am. Chem. Soc.* **127** 10468